J Mater Sci: Mater Electron
DOI 10.1007/s10854-017-7248-0

An effective approach to prepare three-dimensional porous manganese dioxide electrodes by surfactant assisted electrosynthesis for improved supercapacitive properties

Haihan Zhou[1] · Hua-Jin Zhai[1]

Received: 14 February 2017 / Accepted: 29 May 2017

Abstract We report here a simple and effective strategy to promote supercapacitive properties of the MnO_2 electrode, in which sodium dodecyl benzene sulfonate (DBS) as an anionic surfactant is added into the solution used for electrosynthesis. Morphology characterizations indicate that the DBS acts like a pore-forming agent, allowing the deposited MnO_2 nanofibers to form a three-dimensional porous nano-network. The formation mechanism of porous nano-network under DBS assisted electrosynthesis is analyzed accordingly. Electrochemical measurements show that the supercapacitive performance of MnO_2 electrode is effectively enhanced. The MnO_2 electrode prepared with DBS presents a high specific capacitance of 259.7 F g^{-1} at 1 A g^{-1}, which is increased by 30.9% with respect to 198.3 F g^{-1} for the electrode prepared without DBS. Notably, the cycle stability of MnO_2 electrode is significantly improved due to the addition of DBS, which retains 91.0% of its initial capacitance for 2500 cycles. In contrast, the MnO_2 electrode prepared without DBS only maintains 48.7%. The improved properties should promote the applications of MnO_2 in electrochemical capacitors.

✉ Haihan Zhou
hhzhou@sxu.edu.cn

✉ Hua-Jin Zhai
hj.zhai@sxu.edu.cn

[1] Institute of Molecular Science, Key Laboratory of Materials for Energy Conversion and Storage of Shanxi Province, Key Laboratory of Chemical Biology and Molecular Engineering of Education Ministry, Shanxi University, Taiyuan 030006, China

1 Introduction

Supercapacitors have attracted intense attentions due to their high power density, longer cycle life relative to those of secondary batteries, and higher energy density than conventional dielectric capacitors [1, 2]. It is well known that electrode materials are a key factor that determines the performance of a supercapacitor. Among the electrode materials for supercapacitor applications, MnO_2 has been extensively investigated because of its high theoretical specific capacitance, low cost, and environmental friendliness [3]. However, the supercapacitive performance of MnO_2 is limited by its compact morphology and poor electrical conductivity [4]. To this end, recent efforts have been made to improve its electrochemical performance, such as developing different methods (vacuum-assisted filtration [5], chemical bath deposition [6], and sol–gel template synthesis [7]) to prepare MnO_2 with various nanostructures, or incorporating other electrode materials such as Co_3O_4, graphene, and polyaniline into MnO_2 to form nanocomposites [8–10].

Among the preparation methods of MnO_2, electrochemical synthesis shows some advantages. It is easy to handle under mild conditions, simple in adjusting the influence factors, and binder free. However, different process parameters of electrodeposition, including deposition solutions and parameters, have direct influence on the surface morphology and the electrochemical properties of MnO_2 as prepared. Chuang et al. [11] investigated the effect of pH values of the deposition solution on the morphology, Li et al. [12] studied the influence of the Mn-based precursor solutions on the electrochemical performance, and Ali et al. [13] compared the difference of potentiostatic and galvanostatic deposition modes on the structural and electrochemical properties.

Published online: 01 June 2017

Owing to their unique amphiphilic structures, surfactants are known to be capable of significantly reducing the surface energy and surface tension of nanoparticles. The steric effect of surfactant possessing long molecular chains can prevent them from getting together. More importantly, surfactants in solutions can be utilized as templates to facilitate the regulation and control of morphology and structures of materials [14, 15]. Recently, there have been a number of reports on the use of surfactants in the preparation of electrode materials for supercapacitors. Zhang et al. [16] prepared MnO_2 hollow nanospheres by liquid co-precipitation in the presence of cationic surfactant CTAB. Zhou et al. [17] used non-ionic surfactant F127 to enhance the mesoporosity of carbon aerogel for electric double layer capacitor application. In the previous study, we showed that the use of surfactant SDS obviously changes the morphology of electropolymerized conducting polymer [18]. Based on these inspirations, we speculate that the addition of surfactant into the deposition solution may facilitate the change of compact surface morphology of electrodeposited MnO_2 and hence improve its supercapacitive performance.

In this contribution, we choose a new anionic surfactant, sodium dodecyl benzene sulfonate (DBS), for electrodeposition of MnO_2. We report on the comparative findings regarding the morphologies and electrochemical properties of MnO_2 deposited under conditions with and without DBS. Meanwhile, the corresponding mechanism is discussed.

2 Materials and methods

2.1 Fabrication of MnO_2 electrodes

$Mn(CH_3COO)_2{\cdot}4H_2O$ and DBS were of analytical grade. The electrosynthesis was performed with a three-electrode cell, in which a piece of smooth graphite paper (1 cm × 1 cm of conductive area) acted as the working electrode, a Pt foil with large area and a saturated calomel electrode (SCE) were used as the counter electrode and reference electrode, respectively. To remove surface defects and contamination, before use, the graphite paper serving as working electrode was etched in a 20 wt% H_2SO_4 solution for 1 min, and dipped into acetone for 30 s successively. After that, it was cleaned with deionized water and dried in a vacuum oven at 60 °C for several hours.

MnO_2 was electrodeposited on the graphite paper through a constant potential of 0.6 V versus SCE with an optimal deposition time of 5 min, the aqueous deposition solution was composed of 0.1 M $Mn(CH_3COO)_2$ with or without 0.01 M DBS, respectively. The mass of MnO_2 was determined by the weight difference of graphite paper before and after electrodeposition, using a MS105DU Mettler–Toledo microbalance with an accuracy of 10 μg. To ensure weighing the MnO_2 accurately, the graphite paper was dried in the dry oven for 1 h at 60 °C after the deposition. The loading mass of MnO_2 electrodeposited with and without DBS was 0.14 and 0.12 mg cm^{-2}, respectively.

2.2 Characterizations

The samples were characterized by the FT-IR spectra (Bruker Tensor 27 FT-IR Spectrometer), XRD (Rigaku Ultima IV X-ray diffractometer), SEM (JSM-6701F, JEOL), and TEM (JEM-2100, JEOL), respectively. For the FT-IR, XRD, and TEM characterizations, the samples were scraped from the deposit-coated conducting glasses, because it would scrape off the graphite when scraping from the surface of the deposit-coated graphite paper. Electrochemical performances of MnO_2 electrodes were tested by an electrochemical workstation (CHI 660E, Chenhua) with two-electrode system, which consists of two pieces of identical MnO_2 deposited graphite paper electrodes, using a sandwiched filter paper soaked with 1.0 M KCl aqueous solution as the separator. The cyclic voltammetry (CV) and galvanostatic charge/discharge (GCD) were performed between potentials of −0.5 to 0.5 V. Electrochemical impedance spectroscopy (EIS) were recorded at open circuit potential using 5 mV (rms) AC sinusoid signal, and the data were collected in the frequency range of 10^5 to 0.01 Hz.

3 Results and discussion

3.1 Composition and structure

Figure 1a presents the FT-IR spectra of MnO_2 prepared with and without DBS. The spectra are consistent with each other for most of the characteristic peaks. The broadband at 3438 cm^{-1} and absorption at 1630 cm^{-1} are ascribed to the stretching and bending vibrations of physically adsorbed water or crystal water, respectively, whereas the absorptions at around 746 and 521 cm^{-1} can be attributed to Mn–O vibrations of the MnO_6 octahedra in α-MnO_2 [19, 20]. In comparison to the "without DBS" spectrum, additional peaks appear at 1010, 1040, 1125, and 1170 cm^{-1} in the box for the "with DBS" spectrum, which are due to the S–O vibration of DBS used in its preparation process [21, 22]. This observation clearly indicates that for the MnO_2 prepared in the presence of DBS, the MnO_2 sample indeed contains DBS, which is anticipated to affect its morphology and electrochemical properties; see below.

Figure 1b shows the XRD patterns of MnO_2 prepared with and without DBS. It can be seen that they display the

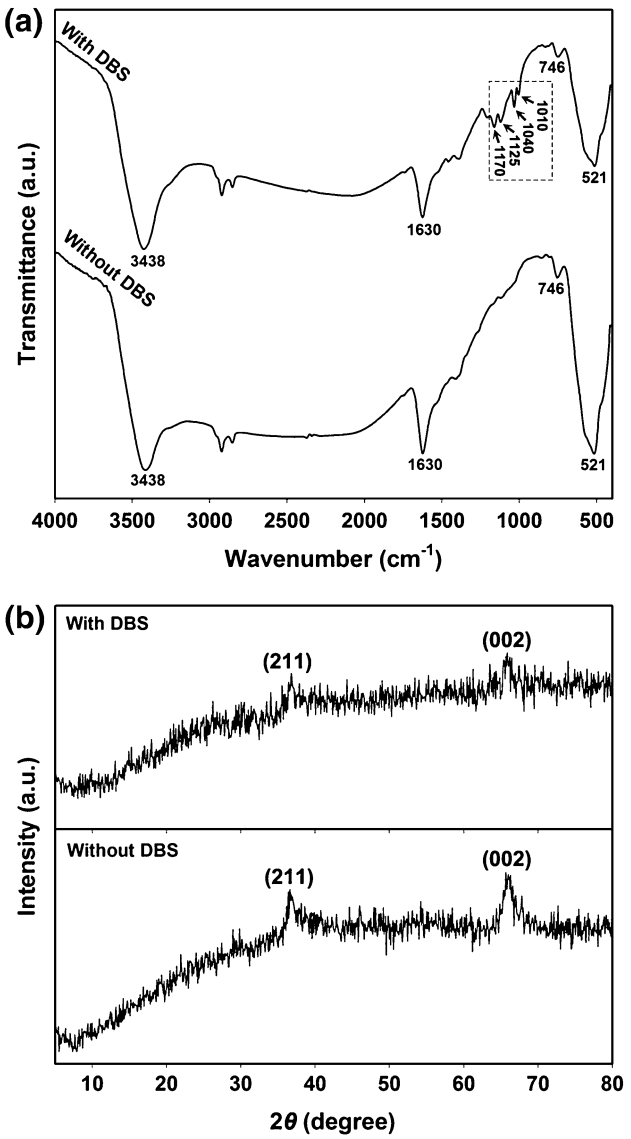

Fig. 1 FT-IR spectra (**a**) and XRD patterns (**b**) of the MnO_2 prepared with and without DBS

same characteristic peaks, suggesting that the addition of DBS in the preparation has no effect on the crystalline phase of MnO_2. The diffraction peaks located at $2\theta = 37°$ (211 plane) and 65.6° (002 plane) can be indexed to α-MnO_2 (JCPDS Card No. 44-0141) [23]. The intensity of diffraction peaks are weak and broad, indicative of a small degree of crystallization for the electrodeposited MnO_2. Thereinto, the diffraction peaks are relatively weaker for MnO_2 prepared with DBS, which appears to be due to the fact that such MnO_2 sample contains DBS.

3.2 Morphology

The supercapacitive performance of metal oxides is strongly related to their morphological characters. It can be observed from the SEM images in Fig. 2 (top panels) that both of MnO_2 prepared with and without DBS exhibit the morphology of sheet-like arrays of nanofibers. However, it is clear that the "with DBS" MnO_2 shows the morphology more like looser and dispersed nanofibers, while the "without DBS" MnO_2 presents the morphology more like compact and stacked nanosheets. The sheet-like arrays of nanofibers of MnO_2 prepared with DBS are crosslinked, loose, and dispersed, forming a three-dimensional porous nano-network. This morphology will facilitate the increase of contact area of MnO_2 with electrolyte and shorten the diffusion path of electrolyte, which benefit the supercapacitive performance.

TEM images can show the morphological details more clearly for the resulting MnO_2. As shown in Fig. 2 (bottom panels), obviously more MnO_2 nanosheets aggregate together for the "without DBS" MnO_2, resulting in darker color, while relatively loose nanosheets can be observed for the "with DBS" MnO_2. In short, the morphology characterizations indicate that the surfactant DBS assisted electrosynthesis can reduce the agglomeration of MnO_2 nanosheets and make them more dispersed and porous.

3.3 Formation mechanism

The formation mechanism of MnO_2 with or without DBS is relatively simple. As illustrated in Fig. 3, when Mn^{2+} ions diffuse to the electrode surface, the MnO_2 film is formed by the oxidation of Mn^{2+} to Mn^{4+}. Thus a compact film is expected in absence of DBS. However, after adding amphiphilic molecules DBS into the deposition solution, the negative charged head groups of DBS are readily adsorbed on the anode surface, whereas the hydrophobic chains are repelled from the electrode surface. The adsorbed DBS may cover parts of the electrode surface, hindering the Mn^{2+} ions from accessing the corresponding areas of the electrode surface. Therefore, the surfactant DBS acts like a pore-forming agent and the deposited film has macropores distributing throughout its entirety, forming a three-dimensional porous nano-network. This also testifies to the fact that DBS are incorporated effectively into the MnO_2 prepared with DBS, as revealed from the FT-IR spectroscopy (Fig. 1a).

3.4 Electrochemical properties

In this study, the supercapacitive properties of the as-prepared MnO_2 samples were investigated using two-electrode cells, which allow a good estimation of the electrode

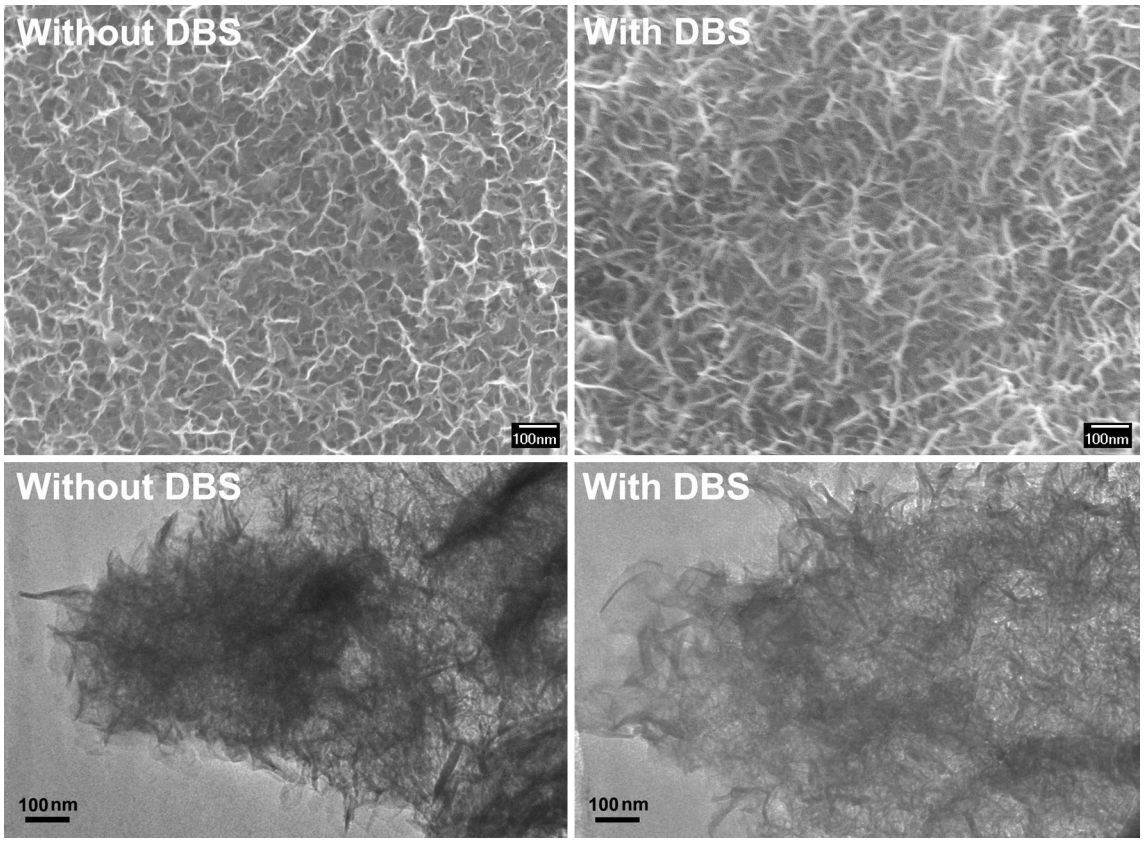

Fig. 2 SEM (*top* panels) and TEM (*bottom panels*) images of the MnO_2 prepared with and without DBS

materials for practical use [24]. Figure 4a shows the CV curves at 10 mV s^{-1} of MnO_2 electrodes prepared with and without DBS. The curve of "with DBS" exhibits the shape that is closer to rectangular, as well as larger area than that of "without DBS", indicating better supercapacitive behavior for the electrode prepared with DBS. Note that the CV curves of MnO_2 electrodes do not show obvious redox peaks, which is because the electrochemical measurements were carried out with a two-electrode system assembled by two pieces of symmetric MnO_2 electrodes. During the tests, one was oxidized and the other reduced, resulting in the redox peaks of MnO_2 being unobvious. Furthermore, it can be seen from Fig. 4b that the CV curves of "with DBS", ranging from 50 to 200 mV s^{-1}, systematically show larger areas than those of "without DBS". The current obviously increases with the adding of scan rate and rectangle-like shapes of CV curves can be observed up to 200 mV s^{-1} for the "with DBS" MnO_2 electrode, manifesting its superior rate capability.

Figure 4c exhibits the GCD curves of MnO_2 electrodes prepared with and without DBS at the current density of 2 A g^{-1}. It can be observed that both types of electrodes exhibit triangular-shape charge/discharge curves, but the electrode prepared with DBS shows longer discharge time and lower IR drops produced by the internal resistance of electrodes than those of "without DBS" electrode. Note that the low internal resistance is a key factor for supercapacitors, because it will be beneficial to decrease the produce of unwanted heat during the charging/discharging processes. Furthermore, the columbic efficiency (η) of electrodes can be determined by calculating the ratio of discharge time t_d to charge time t_c based on the GCD curves. The results calculated manifest the η of "with DBS" electrodes is 91.5%, which is higher than 87.2% of "without DBS" electrodes. The specific capacitance of MnO_2 electrode can be calculated based on GCD curves using the following equation: $C_m = (2\times I\times t)/(m\times \Delta V)$, where C_m (F g^{-1}) is the specific capacitance of the electrode, I (A) the discharge current, t (s) the discharge time, m (g) the mass of electroactive materials, and ΔV (V) the potential window. Figure 4d demonstrates that "with DBS" electrode delivers higher specific capacitance than "without DBS" electrode at various GCD current densities. The resulting MnO_2 electrode prepared with DBS presents a high specific capacitance of 259.7 F g^{-1} at 1 A g^{-1}, which is increased by 30.9% relative to 198.3 F g^{-1} for "without DBS" electrode. Moreover, the electrode prepared with DBS retains 46.2% of initial capacitance when the current density increases from 1 to

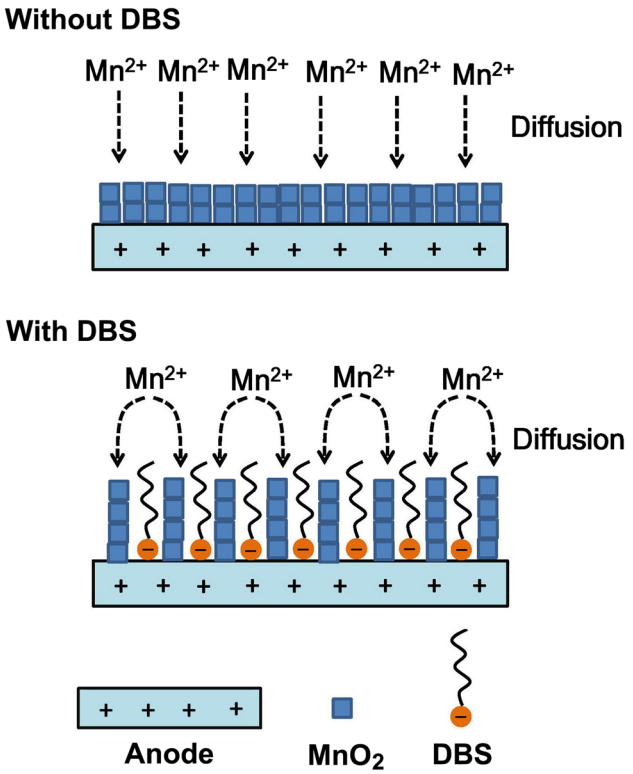

Fig. 3 A schematic illustration for the formation mechanism of the MnO_2 electrodes prepared with and without DBS

20 A g^{-1}, which is higher than 34.3% of "without DBS" electrode, demonstrating that the addition of DBS enhances the rate capability of the electrode prepared. As shown in morphology characterizations, the enhanced electrochemical performance of MnO_2 prepared with DBS can be attributed to its dispersed and porous microstructures due to the introduction of DBS during the process of preparation, which increases the contact area of MnO_2 with electrolyte and shortens the diffusion path of electrolyte.

Figure 5 illustrates the Nyquist plots of the MnO_2 electrodes prepared with and without DBS. Compared with the "without DBS" electrode, the straight line in low frequency region for the "with DBS" electrode leans more towards the imaginary axis, indicating better capacitive behavior [25, 26]. The equivalent series resistance (ESR) can be obtained from the intercept of the curve at the *x*-axis, which mainly arises from the electrolyte, the intrinsic resistance of active materials, and the contact resistance at the interface between current collector and active materials. The inset of Fig. 5 shows that the intercept at x-axis for "with DBS" electrode (5.0 Ω) is smaller than that of "without DBS" electrode (9.3 Ω), that is, the former has a smaller ESR. Low ESR is important for electrochemical capacitors, because it contributes to the reduction of unwanted heat produced during the charging/discharging [27].

To further compare the electrode processes for the two types of electrodes, the knee frequency (f_{knee}) is introduced. As marked in the inset of Fig. 5, it is the maximum frequency at which predominant capacitive behavior can be maintained, which is determined by the crossing of Warburg-type line (inclined 45°) and low-frequency vertical line. Higher knee frequency means faster charge transfer rates and lower ionic diffusion impedance [28, 29]. We can see that the "with DBS" electrode exhibits a higher f_{knee} (6.6 Hz) than the "without DBS" MnO_2 electrode (3.1 Hz). This further indicates that the "with DBS" electrode has better charge transfer and ion diffusion of electrolyte, which will facilitate the rapid charge/discharge performance. Likewise, EIS tests indicate that the introduction of DBS during electrodeposition effectively boosts the supercapacitive performance of the MnO_2 electrode.

3.5 Cycle stability

In addition to poor electrical conductivity, another important issue of MnO_2 is its poor electrochemical cyclability. Herein, a test of 2500 CV cycles at 80 mV s^{-1} was carried out to investigate the stability of electrodes, as shown in Fig. 6. It is observed that the "without DBS" electrode displays a large decline, only maintaining 48.7% of its initial capacitance. Remarkably, the "with DBS" electrode shows a far smoother decline trend, retaining 91.0% of the initial capacitance after 2500 CV cycles. The corresponding reasons are as follows.

The dissolution of MnO_2 into the electrolyte during the tests of cycle stability is believed to be the main cause of capacitance loss of MnO_2 electrodes [12, 30]. An effective route to prevent MnO_2 from electrochemical dissolution is to introduce an effective barrier to Mn cation permeation while allowing the electrolyte to be accessible [31]. In our investigation, the introduced DBS with long alkyl chain probably plays the role of an effective barrier to protect MnO_2 from dissolution during electrochemical cycling. The other possible reason is that the "with DBS" electrode has enhanced capacity for depolarization due to faster charge transfer rate and lower ionic diffusion impedance (as shown in EIS), which result in less dissolution of MnO_2 into the electrolyte. Consequently, the cycle life of the "with DBS" electrode is effectively extended. The cycle stability tests also demonstrate that the DBS surfactant assisted electrosynthesis is a mild and effective method to improve the supercapacitive performance of MnO_2.

4 Conclusions

In summary, an easy and feasible method has been demonstrated to promote the supercapacitive performance of

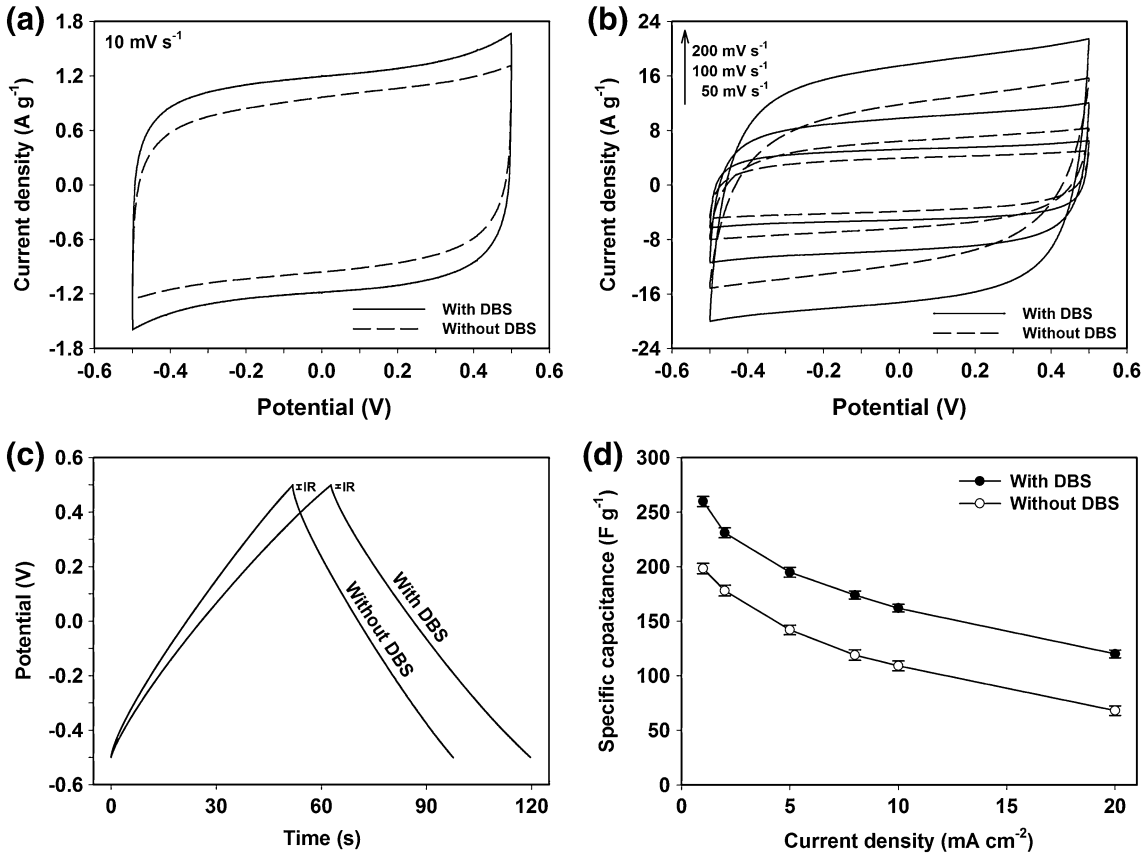

Fig. 4 CV curves at the scan rates of 10 mV s^{-1} (**a**) and 50 to 200 mV s^{-1} (**b**), GCD curves at the current density of 2 A g^{-1} (**c**), and the plots of specific capacitance versus GCD current density (**d**) for the MnO_2 electrodes prepared with and without DBS. Data presented in (**d**) are the mean values along with their standard errors of the mean (n = 3 for each type)

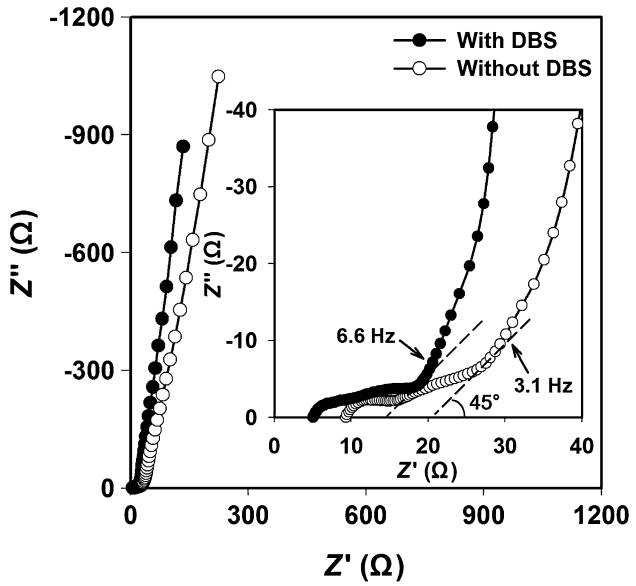

Fig. 5 EIS complex plane plots of the MnO_2 electrodes prepared with and without DBS. The *inset* is their EIS plots in the high-frequency region

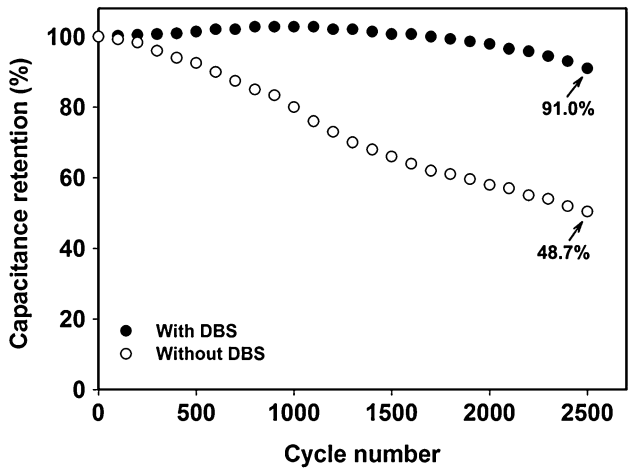

Fig. 6 Capacitance retention as a function of cycle number for the MnO_2 electrodes prepared with and without DBS

MnO_2 electrode by adding DBS surfactant into the solution for electrosynthesis. With the assistant of DBS, the morphology of electrodeposited MnO_2 is changed obviously,

the supercapacitive performance enhanced, and the cycle life extended. Thereinto, the MnO_2 electrode prepared with DBS achieves the specific capacitance of 259.7 F g^{-1} at 1 A g^{-1}, which is increased by 30.9% relative to 198.3 F g^{-1} for "without DBS" electrode. Also its cycle stability is promoted to 91.0% of its initial capacitance for 2500 cycles. These findings should well promote the applications of MnO_2 in supercapacitors. Furthermore, the surfactant assisted method we have developed herein may be further extended to prepare other metal oxides for enhanced supercapacitive performance.

Acknowledgements This work was supported by the National Natural Science Foundation of China (21601113 and 21573138), the Natural Science Foundation of Shanxi Province (2015021079), and China Postdoctoral Science Foundation (2015M571283).

References

1. M. Boota, B. Anasori, C. Voigt, M.Q. Zhao, M.W. Barsoum, Y. Gogotsi, Adv. Mater. **28**, 1517–1522 (2016)
2. M.M. Wu, Y.R. Li, B.W. Yao, J. Chen, C. Li, G.Q. Shi, J. Mater. Chem. A **4**, 16213–16218 (2016)
3. J.Y. Cao, X.H. Li, Y.M. Wang, F.C. Walsh, J.H. Ouyang, D.C. Jia, Y. Zhou, J. Power Sources **293**, 657–674 (2015)
4. S.X. Deng, D. Sun, C.H. Wu, H. Wang, J.B. Liu, Y.X. Sun, H. Yan, Electrochim. Acta **111**, 707–712 (2013)
5. Y. Yu, Y. Zhai, H. Liu, L. Li, Mater. Lett. **176**, 33–37 (2016)
6. Y. Tian, Z.Y. Liu, R. Xue, L.P. Huang, J. Alloy Compd. **671**, 312–317 (2016)
7. X.Y. Wang, X.Y. Wang, W.G. Huang, P.J. Sebastian, S. Gamboa, J. Power Sources **140**, 211–215 (2005)
8. M. Jiang, N. Abushrenta, X.C. Wu, Y.P. Li, X.M. Sun, J. Mater. Sci. **28**, 1281–1287 (2017)
9. S.K. Park, D.H. Suh, H.S. Park, J. Alloy. Compd. **668**, 146–151 (2016)
10. S.N. Fu, L. Ma, M.Y. Gan, S.Y. Wang, X.L. Zhang, J. Zhang, T. Zhou, H.H. Wang, J. Mater. Sci. **28**, 3621–3629 (2017)
11. P.Y. Chuang, C.C. Hu, Mater. Chem. Phys. **92**, 138–145 (2005)
12. W.Y. Li, J.N. Xu, Y.S. Pan, L. An, K.B. Xu, G.J. Wang, Z.S. Yu, L. Yu, J.Q. Hu, Appl. Surf. Sci. **357**, 1747–1752 (2015)
13. G.A.M. Ali, M.M. Yusoff, Y.H. Ng, H.N. Lim, K.F. Chong, Curr. Appl. Phys. **15**, 1143–1147 (2015)
14. L. Huang, H.J. Hou, B.C Liu, K. Zeinu, X.Q. Yuan, X.L. Zhu, X.L. He, L.S. Wu, J.P. Hu, J.K. Yang, Ceram. Int. **43**, 3080–3088 (2017)
15. M.S. Wu, M.J. Wang, Chem. Commun. **46**, 6968–6970 (2010)
16. H.H. Zhang, Y.Q. Wang, C.W. Liu, H.T. Jiang, J. Alloy Compd. **517**, 1–8 (2012)
17. J.H. Zhou, Y.J. Ji, J.P. He, C.X. Zhang, G.W. Zhao, Micropor. Mesopor. Mater. **114**, 424–430 (2008)
18. H.H. Zhou, G.Y. Han, D.Y. Fu, Y.Z. Chang, Y.M. Xiao, H.J. Zhai, J. Power Sources **272**, 203–210 (2014)
19. H.E. Wang, D. Qian, Mater. Chem. Phys. **109**, 399–403 (2008)
20. T. Gao, M. Glerup, F. Krumeich, R. Nesper, H. Fjellvag, P. Norby, J. Phys. Chem. C **112**, 13134–13140 (2008)
21. Y.Y. Xu, S. Yang, G.Y. Zhang, Y.Q. Sun, D.Z. Gao, Y.X. Sun, Mater. Lett. **65**, 1911–1914 (2011)
22. A. Varesano, A. Aluigi, C. Tonin, F. Ferrero, Fibers Polym. **7**, 105–111 (2006)
23. Y.Q. Zhao, D.D. Zhao, P.Y. Tang, Y.M. Wang, C.L. Xu, H.L. Li, Mater. Lett. **76**, 127–130 (2012)
24. V. Khomenko, E. Frackowiak, F. Béguin, Electrochim. Acta **50**, 2499–2506 (2005)
25. H.H. Zhou, G.Y. Han, Y.M. Xiao, Y.Z. Chang, H.J. Zhai, J. Power Sources **263**, 259–267 (2014)
26. C. Peng, J. Jin, G.Z. Chen, Electrochim. Acta **53**, 525–537 (2007)
27. M. Jin, Y.Y. Liu, Y.L. Li, Y.Z. Chang, D.Y. Fu, H. Zhao, G.Y. Han, J. Appl. Polym. Sci. **122**, 3415–3422 (2011)
28. Y. Song, J.L. Xu, X.X. Liu, J. Power Sources **249**, 48–58 (2014)
29. H.H. Zhou, H.J. Zhai, G.Y. Han, J. Power Sources **323**, 125–133 (2016)
30. J. Yan, E. Khoo, A. Sumboja, S.P. Lee, ACS Nano **4**, 4247–4255 (2010)
31. W.F. Wei, X.W. Cui, W.X. Chen, D.G. Ivey, Chem. Soc. Rev. **40**, 1697–1721 (2011)